

# Panoptic-based Object Style-Align for Image-to-Image Translation

Liyun Zhang, Photchara Ratsamee, Bowen Wang, Manabu Higashida, Yuki Uranishi, Haruo Takemura  
Osaka University, Japan

liyun.zhang@lab.ime.cmc.osaka-u.ac.jp

{photchara,uranishi}@ime.cmc.osaka-u.ac.jp      bowen.wang@is.ids.osaka-u.ac.jp

{manabu,takemura}@cmc.osaka-u.ac.jp

## Abstract

Despite remarkable recent progress in image translation, the complex scene with multiple discrepant objects remains a challenging problem. Because the translated images have low fidelity and tiny objects in fewer details and obtain unsatisfactory performance in object recognition. Without the thorough object perception (i.e., bounding boxes, categories, and masks) of the image as prior knowledge, the style transformation of each object will be difficult to track in the image translation process. We propose panoptic-based object style-align generative adversarial networks (POSA-GANs) for image-to-image translation together with a compact panoptic segmentation dataset. The panoptic segmentation model is utilized to extract panoptic-level perception (i.e., overlap-removed foreground object instances and background semantic regions in the image). This is utilized to guide the alignment between the object content codes of the input domain image and object style codes sampled from the style space of the target domain. The style-aligned object representations are further transformed to obtain precise boundaries layout for higher fidelity object generation. The proposed method was systematically compared with different competing methods and obtained significant improvement on both image quality and object recognition performance for translated images.

## 1. Introduction

Image-to-image (I2I) translation is one of the most challenging problems in the field of computer vision. Translated images need to retain the content information of the input domain image and obtain the specific style of the target domain [7]. Several conventional tasks can be considered as I2I translation problems, e.g., super-resolution, neural style transfer, colorization [30]. I2I translation has remarkable recent progress on the improvement of translated image quality (realism and diversity). It has also been adapted

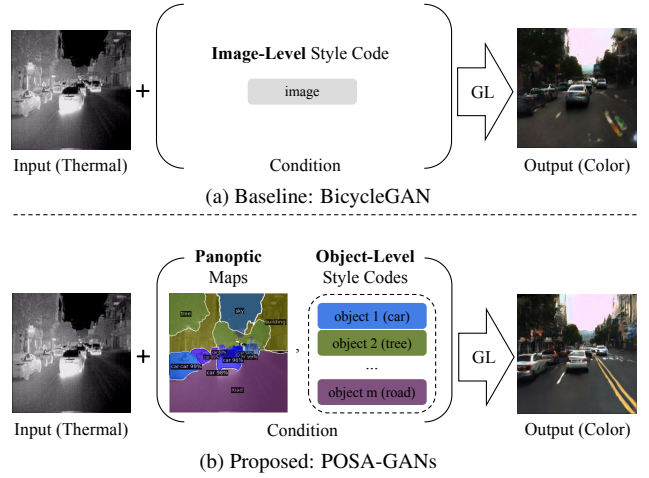


Figure 1. Illustration of pipeline comparison between baseline [43] and our approach for the image-to-image translation; “GL” represents generative learning. (a) shows baseline approach, which uses image-level style code as condition; (b) shows our approach, which uses extracted panoptic maps and object-level style codes with specific objects in the image as conditions.

to image enhancement, such as night-to-day image translation [41] for the improvement of object recognition performance. The pix2pix [9] method was proposed as the first image translation model, which needs paired image datasets for training. CycleGAN [42] and the disentangled representation methods [7, 21, 24] were proposed to be able to support the unpaired dataset training. Pix2PixHD [36] was further proposed to translate more fine-grained and high-resolution images. The attention-based methods [14] can also achieve high-quality image translation by extracting attention regions as image structure guidance.

With the development of image synthesis research based on object perception (e.g., SG2IM [12] synthesizes images from scene and Layout2IM [39] uses layout to achieve the object-level image synthesis), semantics or object instance tends to promote synthesizing the image with sharper ob-

jects. Therefore, some object-level I2I translation methods based on semantics or object instance as a condition have been proposed (*e.g.*, INIT [30] achieves separate learning of instance/local and background/global areas). They can generate high-fidelity object instances.

However, for the complex scene with multiple discrepant objects, the above methods cannot translate images to keep high fidelity and tiny objects in more detail on both foreground and background. Compared with conventional I2I translation which uses image representation as latent code, object-level I2I translation can refine the foreground object instance representation precisely. But it does not fully refine background semantic regions. In contrast, panoptic-level perception extracts overlap-removed foreground object instances (termed “things” in panoptic segmentation) and background semantic regions (termed “stuff” in panoptic segmentation) in the image [17]. It can thoroughly refine each recognizable area in the image for tracking the style transformation during the I2I translation process. Therefore, the results of panoptic-based I2I translation can achieve high fidelity and tiny objects in more details on both foreground and background.

As illustrated in Figure 1 (a), the baseline extracts image representation as content code with image-level style code for I2I translation. Our proposed method utilizes the panoptic segmentation [16] model to extract panoptic-level perception (termed “panoptic maps”) from the image as prior knowledge, which contains object bounding boxes, categories, and masks. In Figure 1 (b), panoptic maps provide bounding boxes for Region of Interest Align (RoIAlign) [5] to extract the object representations as object content codes. The object style codes are sampled from the target style space to align with the content codes for a panoptic-based I2I translation. Our main contributions are threefold:

- **A novel GAN framework with panoptic maps guidance:** The proposed framework uses the panoptic maps of object perception as prior knowledge, which guides the alignment between the object content codes of the input image and the object style codes of the target image. This means that the translated images will have higher fidelity and tiny objects in more detail.
- **A compact panoptic segmentation dataset of thermal domain images and incorporating the Panoptic Quality (PQ) metrics [17] for evaluation:** We annotated a compact panoptic segmentation dataset of thermal images based on the partial KAIST-MS dataset [8]. It is utilized to extract the panoptic maps of thermal images to apply in the inference process of the thermal-to-color image translation task. The PQ metrics are also incorporated to evaluate the object recognition performance of translated images.
- **Extensive performance validation of different methods:** We provide extensive validation for translated images from different methods. The comparison results of both image quality and object recognition performance demonstrate the superiority of our proposed method.

## 2. Related work

**Image-to-image translation.** Image-to-image (I2I) translation models transform the input domain image to the target domain, which changes the style but keeps the scene content unchanged. Pix2Pix [9] achieved paired mapping learning, but it needs the paired datasets and generates single-modal output. BicycleGAN [43] generated multi-mode and more diverse results by encouraging a bijective mapping between the latent and output spaces. CycleGAN [42] achieved unpaired datasets training by using cycle consistency loss. The disentangled representation models [7, 21, 24] utilized a combination of the content from the input domain and the style from the target domain for unsupervised learning. Pix2PixHD [36] can translate high-resolution images by a multi-scale discriminator and coarse2fine generator. AGGAN [35] and U-GAT-IT [14] extracted attention regions as structure guidance to localize important content for a high-quality result. However, for the complex scene with multiple discrepant objects, the above methods cannot generate images in high fidelity.

**Object-level image-to-image translation.** The object-level I2I translation is derived from the development of object-driven image generation research, *e.g.*, synthesizing images from object scenes [1, 12] and synthesizing images from scene layouts [32, 34, 39]. The object-level I2I translation methods utilize object perception (bounding boxes or masks) as guidance, which is effective for generating sharp object boundaries. Instagan [27] incorporated a set of instance attributes for instance-aware I2I translation. DA-GAN [26] learned a deep attention encoder to enable the instance-level correspondences to be discovered consequently. SCGAN [40] and SalG-GAN [10] regarded saliency maps as object perception for object-level I2I translation. Shen *et al.* [30], Su *et al.* [31] and Chen *et al.* [2] combined an object instance-level feature with an image-level feature for a higher quality instance-level I2I translation. However, as these methods only use the instance-level objects (things) without considering the semantic regions (stuff) from the background, the translated images will not have higher fidelity and tiny objects in more details on both foreground and background.

**Panoptic-based image-to-image translation.** From the theoretically reasonable perspective, instance-level I2I translation only considers foreground instances as objects for learning, it will have certain disadvantages compared with panoptic-based I2I translation, which regards both

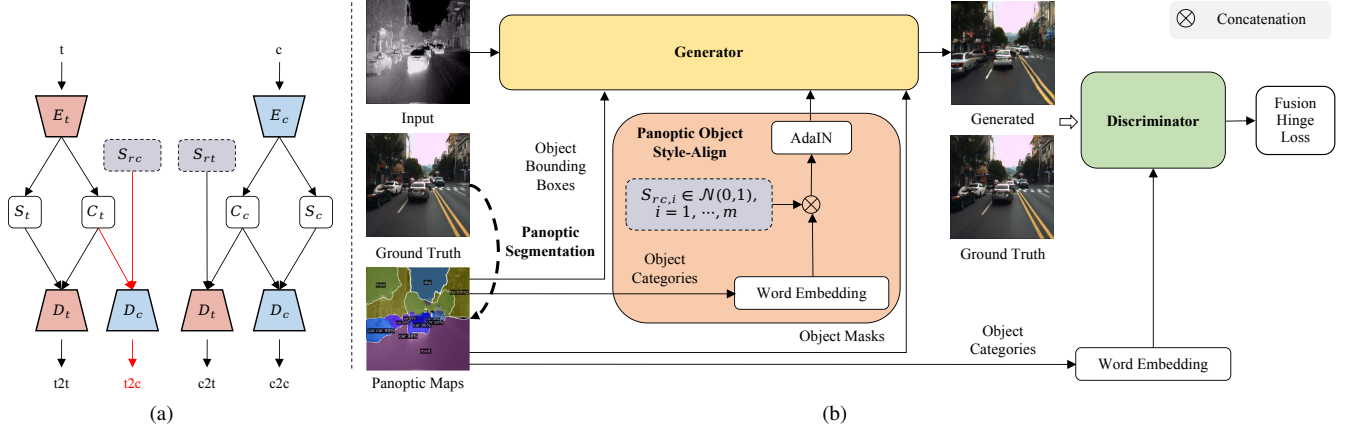


Figure 2. Illustration of the training manner and pipeline for our proposed POSA-GANs. (a) shows the training manner, (b) shows the pipeline. The red arrows in (a) corresponds to the process of (b). The detailed notations are described in the overview section.

foreground things and background stuff as objects for learning. To the best of our knowledge, the panoptic-based I2I translation problem has not yet been investigated. The manner of condition guided I2I translation methods is similar to our work, *e.g.*, Lin *et al.* [23] extracts image regions for the discriminator to improve the performance of GANs and Huang *et al.* [6] provides a solution to control the output based on references semantically. Dundar *et al.* [3] proved that panoptic-level perception guidance makes generated images have higher fidelity and tiny objects in more details for the complex scene with multiple discrepant objects. Panoptic segmentation [17] combines semantic segmentation [25] and instance segmentation [5] to define the uncountable background regions (*e.g.*, sky and road) as stuff and the countable foreground instances (*e.g.*, person and car) as things for thorough region perception of the image. Therefore, we utilize panoptic segmentation to obtain panoptic maps (*i.e.*, things and stuff) of images as prior knowledge, which guides panoptic-based I2I translation for higher fidelity image translation.

### 3. The proposed method

#### 3.1. Overview

We provide an overview of our proposed method from training manner and pipeline, and use the thermal-to-color (transforming thermal domain to color domain) image translation task as an example to describe module details.

**Training manner.** In Figure 2 (a), we use a paired thermal image  $t$  and color image  $c$  from the KAIST-MS [8] dataset to extract content codes (thermal:  $C_t$ , color:  $C_c$ ) and style codes (thermal:  $S_t$ , color:  $S_c$ ).  $E_t$  and  $E_c$  are encoders of  $t$  and  $c$ ;  $D_t$  and  $D_c$  are decoders respectively. By combining  $C_t$  with  $S_t$  to feed into  $D_t$ , we can reconstruct thermal image  $t2t$ . Similarly, combining  $C_c$  with  $S_c$

to feed into  $D_c$ , color image  $c2c$  can be reconstructed. Style codes  $S_{rc}$  and  $S_{rt}$  are randomly sampled from normal distribution. By hypothesizing that  $S_{rc}$  is from the color style space and combining  $C_t$  with  $S_{rc}$  to feed into  $D_c$ , it can translate color image  $t2c$  as indicated by the red arrows. Similarly, we hypothesize that  $S_{rt}$  is from the thermal style space to combine with  $C_c$  to translate the thermal image  $c2t$  by  $D_t$ . For training, the above four processes are divided into cross-domain training ( $t2c$  and  $c2t$ ) and within-domain training ( $t2t$  and  $c2c$ ), which are deployed together.

**Pipeline.** In Figure 2 (b), we utilize the panoptic segmentation model to obtain panoptic maps of the scene, it provides object bounding boxes, categories, and masks as guidance. The RoIAlign [5] in the generator uses bounding boxes to obtain object representations from the input image as object content codes. Style codes  $S_{rc}$  are sampled from a standard Gaussian distribution ( $S_{rc}$  has  $d_{S_{rc}}$  dimensions);  $m$  is the number of objects and equal to the number of objects perceived in the panoptic maps. Note that we treat both things and stuff as objects in panoptic segmentation. We transfer object categories to a multi-dimensional latent vector via word embedding (the dimensional number is  $d_L$ ). It is concatenated with  $S_{rc}$  along the dimension (*i.e.*,  $d_{S_{rc}} + d_L$ ) to combine with the object content codes through Adaptive Instance Normalization (AdaIN) [13] operation. This process achieves panoptic object style-align, which ensures a controllable panoptic-level style transformation. The style-aligned object representations are further refined by object masks to obtain precise boundaries in the generated image layout. The results are composed by convolutional LSTM (cLSTM) [37] following a consistent object sequence perceived by panoptic maps. The translated color images are fed into the discriminator, which combines object categories to calculate object-level loss and image-level loss separately. Here, we utilize fusion hinge loss,

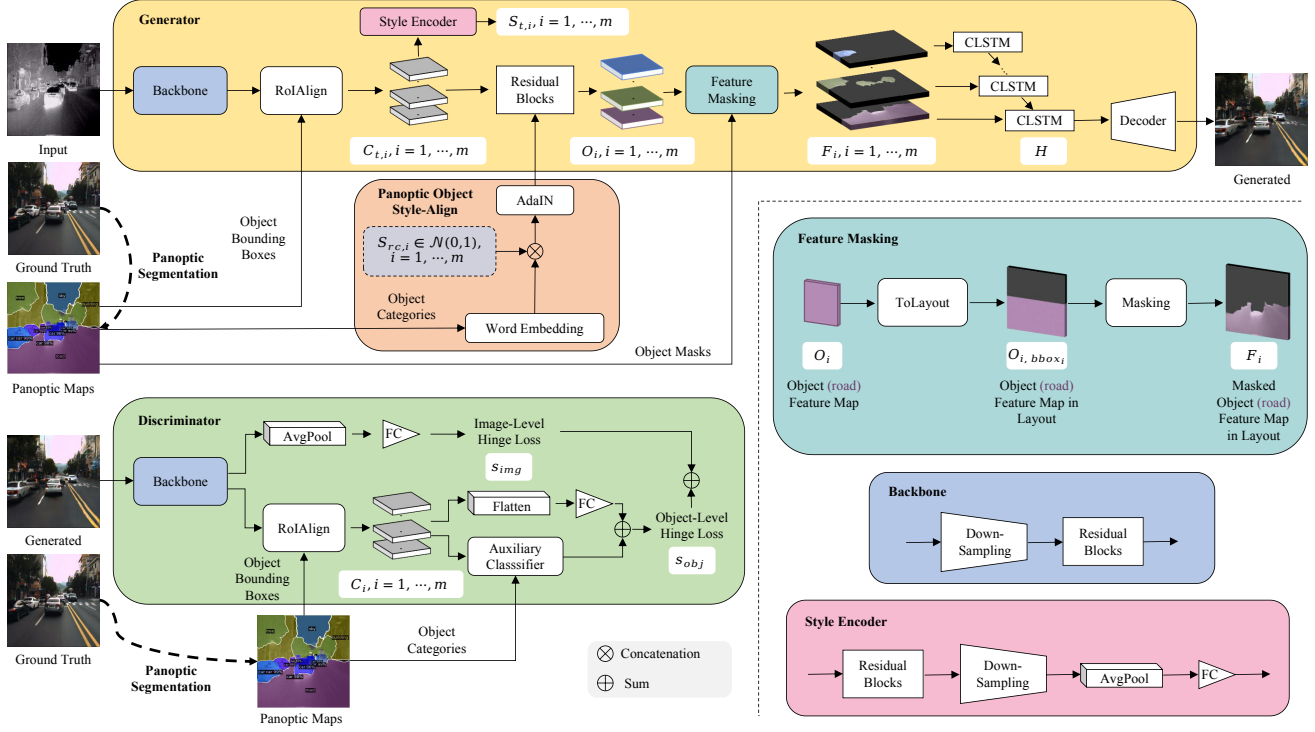


Figure 3. Illustration of the architecture of our proposed POSA-GANs; the detailed notations are described in the architecture section.

which consists of image and object adversarial hinge loss terms [22].

### 3.2. Architecture

#### 3.2.1 Generator

Our architecture, as illustrated in Figure 3, is built upon a generator and discriminator. We deploy a supervised learning setting via paired thermal and color images from the KAIST-MS dataset [8]. Let  $P = \{(category_i, bbox_i, mask_i)_{i=1}^m\}$  be panoptic maps consisting of categories, bounding boxes, and masks, where  $m$  is the number of objects perceived from the panoptic segmentation model and  $category_i \in CAT$  ( $CAT = 134$  in the overlap-removed COCO-Panoptic dataset [17], Things = 80, Stuff = 54, and including the background category). Define  $S_{rc} = \{S_{rc,i}\}_{i=1}^m$  as object style codes randomly sampled from the standard Gaussian distribution. The goal of the generator in the thermal-to-color translation task is to learn a generation function, which is capable of translating thermal image  $t$  to a generated color image  $c'$  via a given condition  $(P, S_{rc})$ :

$$c' = G(t|P, S_{rc}; \Theta_G) \quad (1)$$

where  $\Theta_G$  represents the parameters of the generation function. In our generator  $G(\cdot)$ , the input thermal image  $t$

(size  $256 \times 256$  in the experiment) is first extracted using the backbone module consisting of down-sampling and residual blocks for image representation.

**Panoptic object style-align.** The image representation is cropped by RoIAlign through the object bounding boxes of panoptic maps  $P(bbox_i)_{i=1}^m$  into object representations  $C_t = \{C_{t,i}\}_{i=1}^m$  (size  $8 \times 8$ , dimension  $d_C = 512$ ), where  $C_t$  are object content codes. We utilize a style encoder (as shown in the pink Style Encoder module) to extract object style codes  $S_t = \{S_{t,i}\}_{i=1}^m$  (size  $1 \times 1$ , dimension  $d_S = 256$ ) from  $C_t$ .  $S_t$  will be used in within-domain training of the training manner as described in Figure 2 (a). After this, we use word embedding to make  $P(category_i)_{i=1}^m$  generate latent vectors  $L$  (dimension  $d_L = 256$ ), which are concatenated with  $S_{rc}$  to combine with  $C_t$  through the AdaIN [13] operation for achieving our panoptic object style-align goal.

$$O = (C_t, AdaIN(L, S_{rc})) \quad (2)$$

When we obtained the style-aligned object representation  $O = \{O_i\}_{i=1}^m$  (size  $8 \times 8$ , dimension  $d_C = 512$ ), we utilized a feature masking module to obtain the refined boundaries of object representations.

**Feature masking.** In our feature masking module, we firstly use the "ToLayout" operation to up-sample  $O$  on a



scale  $\alpha$  ( $\alpha = 4$  in our experiment) to balance the object region sizes in the image layout. Because we utilize panoptic maps for object perception, the object region sizes have a gap between things and stuff. Secondly, resized object representations of  $O$  are transformed into their locations (corresponding to  $P(bbox_i)_{i=1}^m$ ; areas outside the bounding boxes are filled with zeros) in the image layout and we obtain  $O_{bbox} = \{O_{i,bbox_i}\}_{i=1}^m$ . To remove background interference information and obtain more precise boundaries of object representations, the masking operation further refines  $O_{bbox}$  by  $M = P(mask_i)_{i=1}^m$  to obtain  $F = \{F_i\}_{i=1}^m$ .

$$F = O_{bbox} \cdot M \quad (3)$$

We feed  $F$  into four layers cLSTM to compose the masked object representations together and obtain fusion image representation  $H$ . Finally, we use a decoder to up-sample  $H$  to generate the translated color image  $c'$ .

### 3.2.2 Discriminator

As illustrated in Figure 3, our discriminator consists of image-level and object-level classifier parts. Similarly to the generator, we first utilize panoptic maps  $P = \{(category_i, bbox_i, mask_i)_{i=1}^m\}$  for guidance. The generated color image  $c'$  is extracted using the backbone module for image representation, which is processed by an image-level classifier consisting of global average pooling and one-output fully convolution (FC) layers to obtain a scalar realness score  $s_{img}$ . The object-level classifier consists of a RoIAlign [5] module, a flatten fully connection layer, a one-output FC layer, and an auxiliary classifier. Image representation is cropped by RoIAlign using the object bounding boxes  $P(bbox_i)_{i=1}^m$  of panoptic maps for object representations  $C = \{C_i\}_{i=1}^m$ . Through flatten and one-output FC layers, we obtain the scalar realness scores for all objects, denoted by  $s_{real} = \{s_{real,obj_i}\}_{i=1}^m$ . We also use the auxiliary classifier to predict the classification scores of all objects combining with  $P(category_i)_{i=1}^m$  word embedding, denoted by  $s_{cls} = \{s_{cls,obj_i}\}_{i=1}^m$ . Therefore, the total average object-level loss is  $s_{obj} = s_{real} + s_{cls}$ . The discriminator will be denoted by  $D(\cdot, \Theta_D)$  with parameters  $\Theta_D$ . Given an image  $I$  (ground truth  $c$  or generated color image  $c'$ ) and condition  $P$ , the discriminator computes the prediction score for the image and the average score for objects.

$$(s_{img}, s_{obj}) = D(I|P; \Theta_D) \quad (4)$$

### 3.3. Loss function

The full objective of our model comprises five loss functions. We train the generator and discriminator networks end-to-end in an adversarial manner. The generator is trained to minimize the weighted sum of losses:

**Adversarial loss.** We utilize the image-level and object-level fusion hinge version [22] of the standard adversarial loss [4] to train  $(\Theta_G, \Theta_D)$  in our POSA-GANs,

$$l_k(I|P) = \begin{cases} \min(0, -1 + p_k); & \text{if } I \text{ is ground truth } c \\ \min(0, -1 - p_k); & \text{if } I \text{ is generated } c' \end{cases} \quad (5)$$

where  $k \in \{img, obj\}$ . Let  $l(I|P) = l_{img}(I|P) + \lambda \cdot l_{obj}(I|P)$  with trade-off parameter  $\lambda$  (1.0 used in our experiments) in fusion hinge losses between image-level and object-level. We define the losses for the discriminator and generator respectively [32],

$$\begin{aligned} L_{adv}(\Theta_D, \Theta_G) &= - \mathbb{E}_{(I|P) \sim p_{all}(I|P)} [l(I|P)] \\ L_{adv}(\Theta_G, \Theta_D) &= - \mathbb{E}_{(I|P) \sim p_{fake}(I|P)} [D(I|P; \Theta_D)] \end{aligned} \quad (6)$$

where minimizing  $L(\Theta_D, \Theta_G)$  tries to tell the discriminator to distinguish the ground truth and translated images, but minimizing  $L(\Theta_G, \Theta_D)$  tries to fool the discriminator by translating fine-grained images.  $p_{all}(I|P)$  represents all of the ground truth and translated images, and  $p_{fake}(I|P)$  represents the translated images.

**Image reconstruction loss.** We need  $L_1^{img} = \|c' - c\|_1$  to penalize the  $L_1$  difference between the translated image  $c'$  and ground truth  $c$ . Here, we mainly calculate the within-domain ( $t2t$  and  $c2c$ ) way.

**KL loss.** We use a style encoder module to extract object style codes  $S_t = \{S_{t,i}\}_{i=1}^m$  of the thermal image. In the cross-domain of  $c2t$ , we also extract the  $S_c = \{S_{c,i}\}_{i=1}^m$  from the color image. Therefore, we use  $L_{kl}$  to compute the KL-Divergence between distributions  $S_t$  and  $S_c$  with normal distribution  $S_{rt}$  and  $S_{rc}$  separately,

$$L_{kl} = \sum_{i=1}^m \mathbb{E} [D_{KL}((S_t, S_c) || (S_{rt}, S_{rc}))] \quad (7)$$

where  $m$  is the number of objects in the panoptic maps.

**Object latent reconstruction loss.** We also re-extract object style codes  $S'_t$  and  $S'_c$  from translated  $c2t$  and  $t2c$ .  $L_1^{latent} = \sum_{i=1}^m \|(S'_t, S'_c) - (S_{rt}, S_{rc})\|_1$  penalizes the  $L_1$  difference between sampled  $S_{rt}$  and  $S_{rc}$  and translated object style codes  $S'_t$  and  $S'_c$ .

**Perceptual loss.** We use  $L_p$  to alleviate the problem that translated images are prone to producing distorted textures [36]. It is beneficial to keep textures in high-level space through the ReLU activation of the VGG-19 network [11],

$$L_p = \sum_k \frac{1}{C_k H_k W_k} \sum_{i=1}^{H_k} \sum_{j=1}^{W_k} \|\phi_k(y)_{i,j} - \phi_k(G(t))_{i,j}\|_1 \quad (8)$$

where  $\phi_k(\cdot)$  represents the feature representations of the  $k$ th max-pooling layer in the VGG-19 network, and  $C_k H_k W_k$  represents the size of feature representations.

**Full objective.** The final loss function is defined as:

$$L_{\text{total}} = \lambda_1 L_{\text{adv}} + \lambda_2 L_1^{\text{img}} + \lambda_3 L_{\text{kl}} + \lambda_4 L_1^{\text{latent}} + \lambda_5 L_p \quad (9)$$

where  $\lambda_i$  are the parameters balancing different losses.

### 3.4. Implementation details

In  $L_{\text{total}}$ , the  $\lambda_1 \sim \lambda_5$  were set to 0.1, 1, 1, 1 and 1. Model parameters were initialized using the Orthogonal Initialization method [29]. For the activation function, we used leaky-ReLU with a slope of 0.2 in modules. We trained our model using the Adam optimizer [15] with  $\beta_1 = 0$  and  $\beta_2 = 0.999$ . The learning rates were set to  $10^{-4}$  for the generator and 0.005 for the discriminator. We set 400,000 iterations for training on four NVIDIA V100 GPUs.

## 4. Experiments

We conducted extensive experiments to evaluate our method with state-of-the-art models of I2I translation tasks to show superiority in aspects of image quality and object recognition performance. For competing methods, Pix2Pix [9], MUNIT [7] and BicycleGAN [43] belong to image-level I2I translation. As INIT [30] has no open implementation code and SCGAN [40] uses a saliency map for object perception, we use SCGAN as object-level I2I translation. TIC-CGAN [19] tends to show superiority on the thermal-to-color translation task. Based on specific metrics, we summarized the image quality and object recognition performance for different methods as qualitative and quantitative results respectively. Note that, discussion of the ablation study and limitations, as well as further experimental results will be provided in the supplementary materials.

### 4.1. Datasets

We train and evaluate our model on the KAIST-MS [8] and Transient Attributes datasets [20] for thermal-to-color and day-to-night tasks respectively using  $256 \times 256$  resolution images. For panoptic maps in the training process of the thermal-to-color task, we utilized the pre-trained Panoptic FPN model [16] based on COCO-Panoptic dataset [17] to perceive from paired color images. For panoptic maps in the inference process, we obtained from the pre-trained Panoptic FPN model on our annotated thermal panoptic segmentation dataset. This dataset has annotated 2,026 pairs of thermal and color images. The raw KAIST-MS dataset (only daytime images) was condensed to 11,610 images for training and 2,541 images for evaluation. In the day-to-night task, we used 17,823 images for training and 2,287 images for evaluation. The panoptic maps in training and

inference processes were all obtained from the pre-trained Panoptic FPN model on daytime images.

### 4.2. Evaluation metrics

We use Human Preference, Inception Score and Diversity Score metrics for image quality, and Panoptic Quality (PQ) [17] series metrics for object recognition performance.

**Human Preference** is a user perceptual study that compares the realism and faithfulness of translated images from different methods. Twenty participants (average age: 29.90, std: 23.49) were shown the translated results (515 images sampled from the evaluation set) from the thermal-to-color task. Participants were asked to select the best image by considering realism, object sharpness and scene similarity, which were calculated together using different weights (0.5, 0.3 and 0.2, respectively) for final comprehensive scores.

**Inception Score** [28] is a popular metric that measures the quality of generated images from GANs. It uses an Inception V3 network pre-trained on the ImageNet-1000 classification benchmark and computes a statistical score of the network’s outputs [33].

**Diversity Score** measures the differences between paired images generated from the same input by computing the perceptual similarity in deep feature space [39]. We used the LPIPS metric [38] for diversity scoring and pre-trained AlexNet [18] for feature extraction.

**Panoptic Quality (PQ)** is adopted to evaluate object recognition performance, PQ combines segmentation quality (SQ) and recognition quality (RQ) [17],

$$PQ = \underbrace{\frac{\sum_{(p,g) \in TP} \text{IoU}(p,g)}{|TP|}}_{\text{segmentation quality (SQ)}} \times \underbrace{\frac{|TP|}{|TP| + \frac{1}{2}|FP| + \frac{1}{2}|FN|}}_{\text{recognition quality (RQ)}} \quad (10)$$

where SQ sums up the intersection over union ratios to evaluate how closely matched predicted segments are with their ground truths. RQ combines precision and recall to identify how effective a trained model is at getting a prediction right.  $PQ^{\text{Th}}$ ,  $SQ^{\text{Th}}$ ,  $RQ^{\text{Th}}$  are used on thing (Th) categories;  $PQ^{\text{St}}$ ,  $SQ^{\text{St}}$ ,  $RQ^{\text{St}}$  are used on stuff (St) categories.

### 4.3. Qualitative results

For image quality, the human preference results in Table 1 show that our approach achieved a significantly higher score in the human perceptual study of the thermal-to-color task compared to other approaches. As translated night images by the day-to-night task are difficult to distinguish by human vision, they were intensively evaluated with quantitative metrics. Figure 4 demonstrates that our POSA-GANs can translate higher fidelity and brightly colored images, and have tiny objects in more details. In contrast, the results of other methods are more blurry, distorted and missing small objects. For translated objects, our results tend

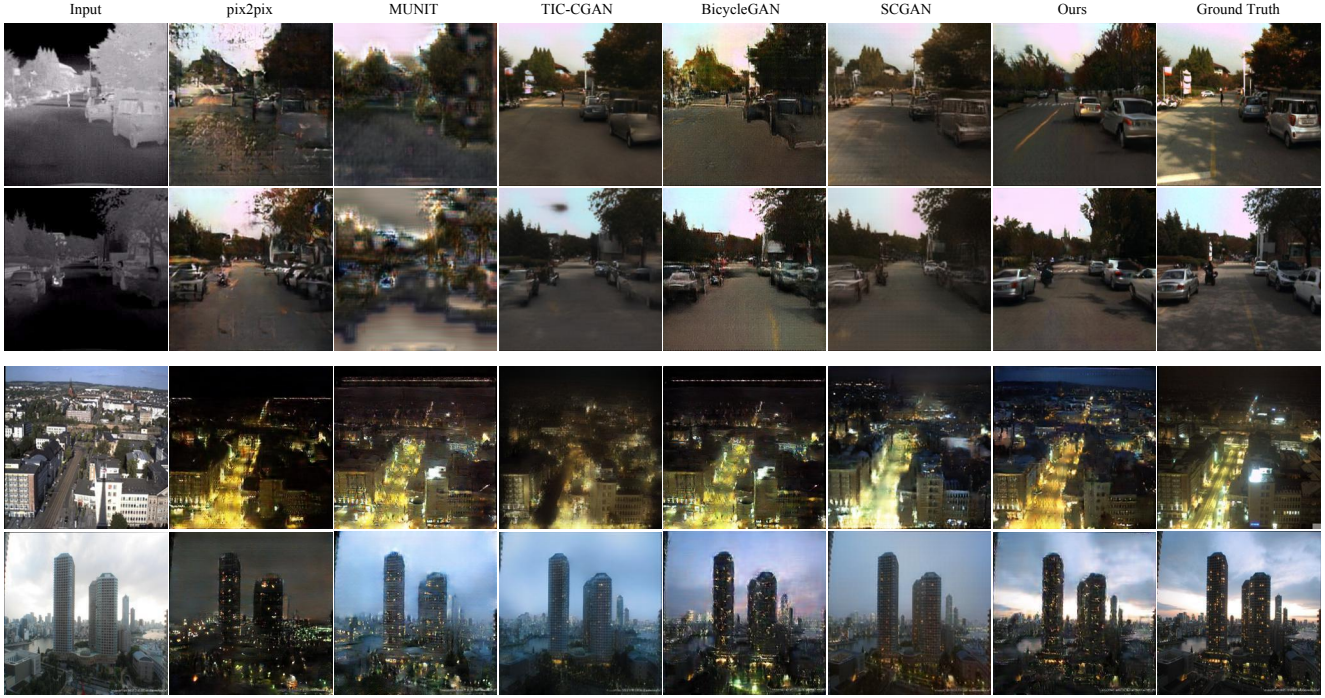


Figure 4. Comparison of the image quality of translated images from different approaches; the upper row group is the result of the thermal-to-color image translation task, and the lower row group is the result of the day-to-night image translation task.

Method	Human Preference	Inception Score		Diversity Score	
	thermal $\rightarrow$ color	thermal $\rightarrow$ color	day $\rightarrow$ night	thermal $\rightarrow$ color	day $\rightarrow$ night
pix2pix [9]	0.39%	$2.29 \pm 0.11$	$1.50 \pm 0.10$	0.46	0.65
MUNIT [7]	0.13%	$1.94 \pm 0.30$	$1.80 \pm 0.22$	<b>0.54</b>	0.65
TIC-CGAN [19]	13.65%	$2.59 \pm 0.50$	$1.62 \pm 0.14$	0.39	0.53
BicycleGAN [43]	10.04%	$2.61 \pm 0.26$	$1.86 \pm 0.21$	0.47	0.60
SCGAN [40]	33.30%	$2.70 \pm 0.56$	$1.22 \pm 0.13$	0.37	0.65
Ours	<b>42.48%</b>	<b><math>2.85 \pm 0.38</math></b>	<b><math>1.90 \pm 0.17</math></b>	0.49	<b>0.67</b>

Table 1. Human Preference, Inception Score and Diversity Score metrics (higher is better) are used to evaluate the image quality of translated images from different methods in thermal-to-color and day-to-night tasks.

better sharpness, more natural color style and display diversity (*e.g.*, the appearance of cars). On the other methods side, object sharpness is not satisfactory, the style is far from the ground truth and there is insufficient diversity. For object recognition performance, we used the panoptic segmentation result by the Panoptic FPN model pre-trained on the COCO-Panoptic dataset. We only show the object recognition results on the thermal-to-color task, because the translated night images from the day-to-night task have disadvantages of insignificant differences for object recognition comparison. Figure 5 shows that our method can achieve better object recognition performance, *e.g.*, the number and boundaries of cars; the structure of the sky, tree and road;

and the areas where there are relatively fewer recognition failures. Moreover, compared with the recognition results of the original thermal image, the results of our translated color images are significantly improved, this also verifies the advantages of our method when adapted for image enhancement.

#### 4.4. Quantitative results

For image quality, the inception score and diversity score in Table 1 show that our approach achieved significantly higher scores than other approaches. Only the diversity score of MUNIT [7] in the thermal-to-color translation task achieved a higher score than our approach, which is be-





Figure 5. The performance of translated images in object recognition for different approaches; in each group, the upper row contains translated images from different approaches, and the lower row is the result of the corresponding object recognition.

Method	PQ	SQ	RQ	PQ <sup>Th</sup>	SQ <sup>Th</sup>	RQ <sup>Th</sup>	PQ <sup>St</sup>	SQ <sup>St</sup>	RQ <sup>St</sup>
pix2pix [9]	3.3	12.1	4.2	0.6	9.6	0.8	9.0	17.5	11.3
MUNIT [7]	1.6	7.2	2.1	0.1	3.3	0.1	3.9	13.4	5.3
TIC-CGAN [19]	5.6	15.2	7.4	1.7	11.8	2.6	13.6	22.5	17.4
BicycleGAN [43]	4.3	16.8	5.5	0.8	13.1	1.2	10.9	23.9	13.6
SCGAN [40]	<b>7.2</b>	<b>19.6</b>	<b>9.0</b>	3.1	15.4	3.9	<b>16.7</b>	<b>29.1</b>	<b>20.9</b>
Ours	6.3	17.6	8.0	<b>3.2</b>	<b>15.5</b>	<b>4.2</b>	12.8	22.0	15.9

Table 2. The PQ, SQ and RQ series metrics (higher is better) are utilized to evaluate the object recognition performance of translated images from different approaches in the thermal-to-color task.

cause MUNIT adds extra noise to the target style space for generating more variant results in the experimental inference process. For object recognition performance, Table 2 shows that our method performs better on PQ, SQ, RQ, PQ<sup>Th</sup>, SQ<sup>Th</sup>, RQ<sup>Th</sup> than other image-level image translation methods (*i.e.*, pix2pix [9], MUNIT [7], TIC-CGAN [19] and BicycleGAN [43]). Although the object-level method (*i.e.*, SCGAN [40]) achieved the best scores in PQ, SQ, RQ, and PQ<sup>St</sup>, SQ<sup>St</sup>, RQ<sup>St</sup>, our method performed best in the PQ<sup>Th</sup>, SQ<sup>Th</sup>, RQ<sup>Th</sup>. This shows that our method can finely separate the unclear object boundary problem in a complex scene with multiple discrepant objects caused by the overlap of things and stuff. In addition, our method achieved lower scores on PQ<sup>St</sup> and RQ<sup>St</sup> than TIC-CGAN, and a lower

score on SQ<sup>St</sup> than TIC-CGAN and BicycleGAN methods. The reason for the above two cases is possible because our method regards both things (foreground objects) and stuff (background regions) in panoptic segmentation as objects; therefore, there is generally a gap between the size of stuff and things. In the experiment, we used a hyper-parameter (scale of 4) of up-sampling for balance, which causes that the results of PQ<sup>St</sup>, SQ<sup>St</sup> and RQ<sup>St</sup>. It shows that the currently trained model is prone to be more sensitive to the performance of things.



## 5. Novelty Comparison

In order to illustrate the novelty of our proposed method more concisely, we compared the image-level image-to-image (I2I) translation, the object-level I2I translation, and our proposed panoptic-based I2I translation frameworks respectively.

**Image-level I2I translation:** this approach uses a content encoder to extract image representation from the original image directly as content code. As illustrated in Figure 6 (a), the style code is sampled from the style space of the ground truth image [43]. They are combined to input decoder for the image-level I2I translation.

**Object-level I2I translation:** this approach uses instance segmentation [5] to perceive the object information (*i.e.*, bounding boxes, categories, and masks) in the original image. In Figure 6 (b), the content encoder uses it to extract object instance representations as content code, and the instance-level style code is also sampled from instance-level style space based on instance perception of ground truth image. The object instances from the input domain and ground truth domain are aligned to achieve precise object-level style transformation [30]. However, the instance perception of object-level I2I translation method only considers foreground object instances (*e.g.*, car, person, which are countable objects termed "things" in panoptic segmentation [17]), and does not consider background semantic regions (*e.g.*, sky, road, which are uncountable objects termed "stuff").

**Panoptic-based I2I translation:** we utilize panoptic segmentation [16] to extract panoptic perception, which considers both things and stuff. As illustrated in Figure 6 (c), compared with object instance-level (things only) style-align of object-level I2I translation, our method can achieve object panoptic-level (things + stuff) style-align. This demonstrates that our method has the superiority of fine object perception and more precise style transformation in the I2I translation process, which can achieve translated images in higher fidelity and tiny objects in more detail in complex scenes with multiple discrepant objects.

## 6. Ablation Study

We demonstrate the necessity of all components of our proposed model by comparing the inception score (IS) [28], diversity score (DS) [39] for image quality, and PQ (Panoptic Quality), SQ (Segmentation Quality), RQ (Recognition Quality) for object recognition performance [17]. They are deployed for the translated images using several ablated versions of our model trained on the KAIST-MS [8] dataset of the thermal-to-color translation task.

As shown in Table 3, removing any loss term will decrease the overall performance. Specifically, the trained model without  $L_1^{\text{img}}$  (image reconstruction loss) or  $L_1^{\text{latent}}$

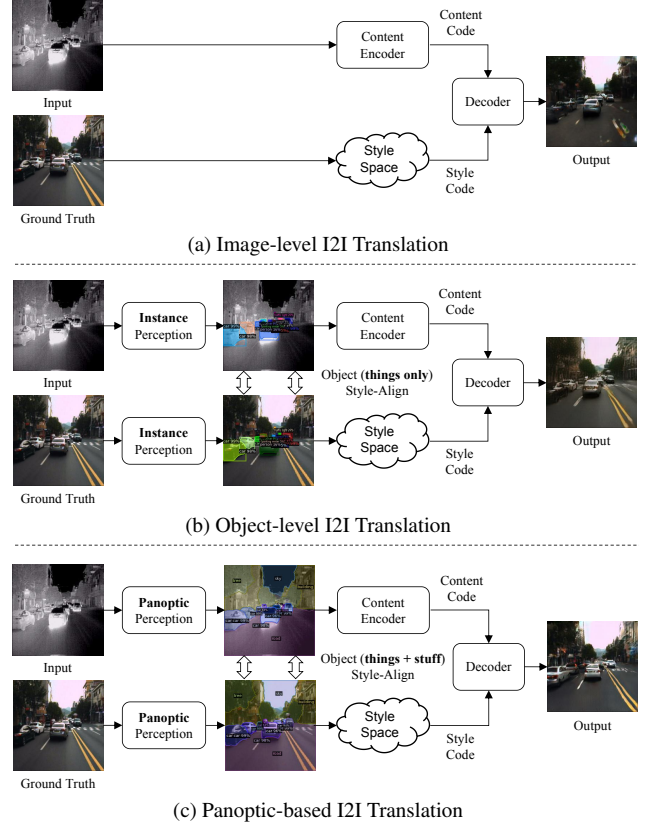


Figure 6. Illustration of comparison for the Image-level image-to-image (I2I) translation, object-level I2I translation and our proposed panoptic-based I2I translation. The details are described in the novelty comparison section.

Method		IS	DS	PQ	SQ	RQ
w/o $L_1^{\text{img}}$		2.64	0.45	3.0	10.7	3.7
w/o $L_1^{\text{latent}}$		2.54	0.43	3.3	11.7	4.1
w/o $L_{\text{kl}}$		2.64	0.45	3.2	10.8	3.9
w/o $L_{\text{adv}}$		2.26	<b>0.56</b>	2.4	7.9	2.9
w/o $L_{\text{p}}$		2.66	0.45	3.3	11.4	4.1
full model		<b>2.85</b>	0.49	<b>6.3</b>	<b>17.6</b>	<b>8.0</b>

Table 3. Ablation study of our model on thermal-to-color translation task by removing different objectives. IS is the inception score, DS is the diversity score, PQ is the panoptic quality, SQ is the segmentation quality, and RQ is the recognition quality.

(object latent reconstruction loss) or  $L_{\text{kl}}$  (KL loss) constraints first translate lower-fidelity images, which decreases the inception scores. Meanwhile, the diversity scores are also decreased, *i.e.*, multiple variation target domain images cannot be translated as same as the full model. The decreased PQ, SQ, and RQ also reflect in low performance of the translated image in object recognition. Re-

moving  $L_{adv}$  (adversarial loss), the translated images by the model have significantly lower inception score and object recognition performance than the full model. Because we adopt the image-level and object-level fusion hinge loss [22], which also contains the object classification for generated objects, the lack of this part will significantly decrease the object recognition performance. As expected, the lack of this part of the constraint results in a higher diversity score. Without  $L_p$  (perceptual loss), the model cannot alleviate the problem that translated images are prone to producing distorted textures. This will inevitably lead to a decrease in both image quality (inception score and diversity score) and object recognition performance (PQ, SQ and RQ), and the results of the table also verified this.

## 7. Limitations

Although our method can achieve a comprehensive improvement on image quality and object recognition performance for translated images compared with different methods, our method still has limitations in some respects.

Firstly, considering the high cost of manually labeling the panoptic segmentation dataset, and in order to learn the direct translation of image-to-image without additional labels (*i.e.*, the panoptic maps are not used as supervised data outside the model), we utilize the pre-trained Panoptic FPN model [16] based on COCO-Panoptic dataset [17] to perceive the panoptic maps in the training process from the input domain images. Also, we use the pre-trained Panoptic FPN model on our annotated thermal panoptic segmentation dataset to perceive the panoptic maps in the inference process. Since the panoptic segmentation performance of the pre-trained model is limited, the experimental results based on this condition will also be decreased to a certain extent.

Secondly, similar to BicycleGAN [43], our method also uses the supervised learning of the paired dataset to train the model. As we need to extract panoptic maps from the image as guidance for model training, it has certain requirements on the dataset, *i.e.*, the input needs to be an image that can achieve object segmentation. Like some classic tasks mentioned in pix2pix [9], *e.g.*, translating labels to the street scene, translating labels to the facade, and translating edges to photo, our method cannot achieve these because their inputs are not images to perceive good enough of object perception.

Finally, as our method uses panoptic segmentation to finely perceive the object instances (things) from the foreground and the semantic regions (stuff) from the background [17] to learn an image translation model, it can achieve a high object-level diversity. For things (*e.g.*, car), the model generates different details, which result in good diversity. However, for stuff (*e.g.*, road), if the generated road texture is highly different from the ground truth (*e.g.*, lane markings and zebra crossings), it will decrease the

whole image quality. This is due to the fact that normally the stuff in the background has a large region, which should be considered with the majority of the whole image context in the image translation process.

## 8. Additional Experiment Results

As shown in Figure 7 and Figure 8, we added more experimental results compared our method with various I2I translation models including pix2pix [9], MUNIT [7], TIC-CGAN [19], BicycleGAN [43], and SCGAN [40]. The results show the evaluation of image quality and object recognition performance for the translated images on the thermal-to-color translation task using different methods respectively.

## 9. Conclusion

We propose a novel panoptic-based object style-align image-to-image translation method together with a compact panoptic segmentation dataset. Our method incorporates the panoptic-level perception to achieve translated images in higher fidelity and tiny objects in more detail in complex scenes with multiple discrepant objects. Extensive experiments demonstrated that our method obtained significant improvement in both image quality and object recognition performance for translated images compared to different methods. Incorporating bounding boxes and mask regression losses in image translation model training will be the focus of our future work.

## 10. Acknowledgments

This work has been partly supported by the KAKENHI Fund for the Promotion of Joint International Research (fostering joint international research (B) No. 20KK0086) and the Mohamed Bin Zayed International Robotics Challenge (MBZIRC) Grant.

## References

- [1] Oron Ashual and Lior Wolf. Specifying object attributes and relations in interactive scene generation. In *Proceedings of the IEEE/CVF International Conference on Computer Vision*, pages 4561–4569, 2019. 2
- [2] Tianlang Chen, Wei Xiong, Haitian Zheng, and Jiebo Luo. Image sentiment transfer. In *Proceedings of the 28th ACM International Conference on Multimedia*, pages 4407–4415, 2020. 2
- [3] Aysegul Dundar, Karan Sapra, Guilin Liu, Andrew Tao, and Bryan Catanzaro. Panoptic-based image synthesis. In *Proceedings of the IEEE/CVF Conference on Computer Vision and Pattern Recognition*, pages 8070–8079, 2020. 3
- [4] Ian Goodfellow, Jean Pouget-Abadie, Mehdi Mirza, Bing Xu, David Warde-Farley, Sherjil Ozair, Aaron Courville, and Yoshua Bengio. Generative adversarial nets. *Advances in neural information processing systems*, 27, 2014. 5





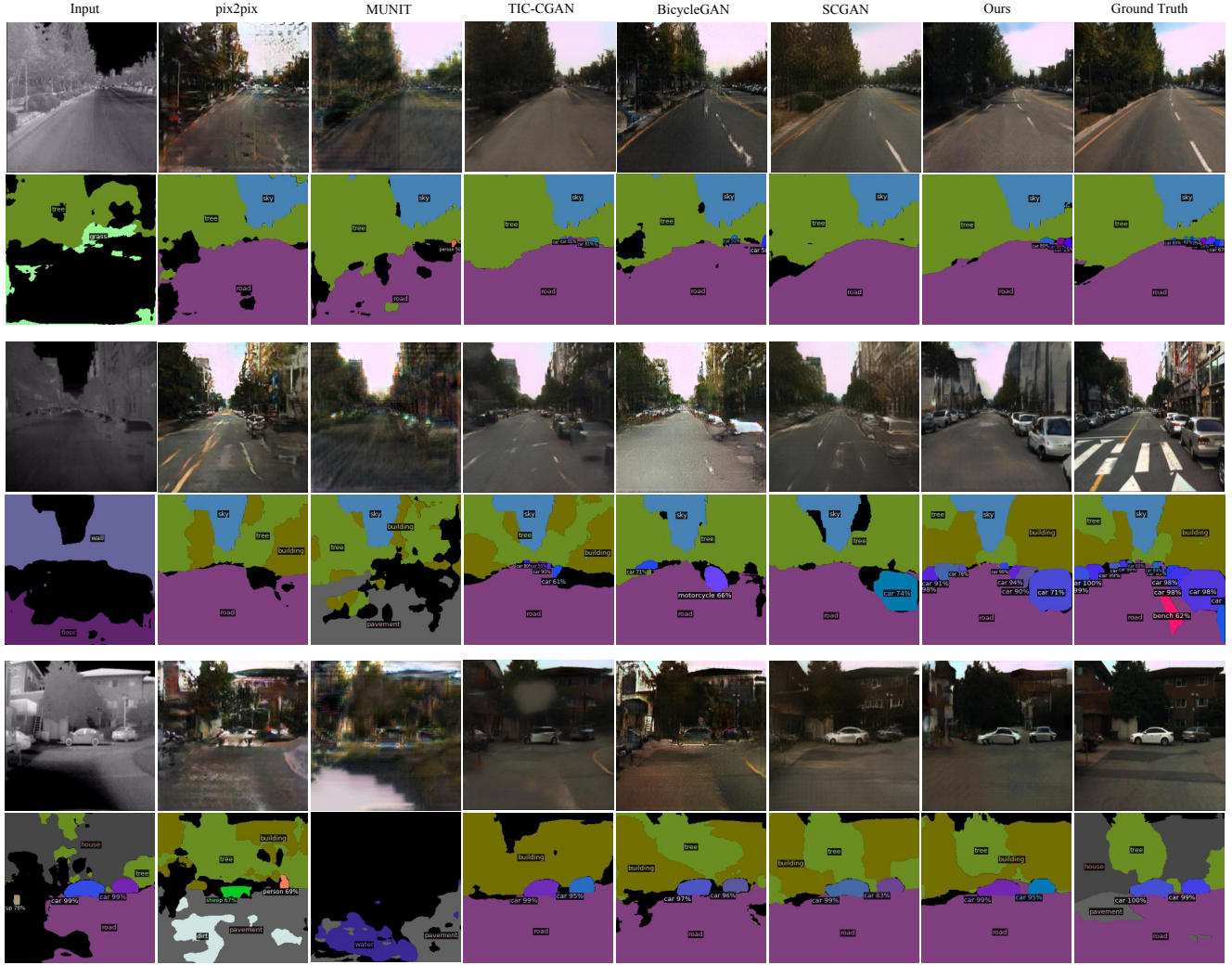


Figure 8. More qualitative results of translated images on the thermal-to-color translation task using different approaches; in each group, **upper row** is the image quality comparisons; **lower row** is the object recognition performance comparison.

- generator architecture for generative adversarial networks. In *Proceedings of the IEEE/CVF Conference on Computer Vision and Pattern Recognition*, pages 4401–4410, 2019. 3, 4
- [14] Junho Kim, Minjae Kim, Hyeonwoo Kang, and Kwanghee Lee. U-gat-it: Unsupervised generative attentional networks with adaptive layer-instance normalization for image-to-image translation. *arXiv preprint arXiv:1907.10830*, 2019. 1, 2
- [15] Diederik P Kingma and Jimmy Ba. Adam: A method for stochastic optimization. *arXiv preprint arXiv:1412.6980*, 2014. 6
- [16] Alexander Kirillov, Ross Girshick, Kaiming He, and Piotr Dollár. Panoptic feature pyramid networks. In *Proceedings of the IEEE/CVF Conference on Computer Vision and Pattern Recognition*, pages 6399–6408, 2019. 2, 6, 9, 10
- [17] Alexander Kirillov, Kaiming He, Ross Girshick, Carsten Rother, and Piotr Dollár. Panoptic segmentation. In *Proceedings of the IEEE/CVF Conference on Computer Vision and Pattern Recognition*, pages 9404–9413, 2019. 2, 3, 4, 6, 9, 10
- [18] Alex Krizhevsky, Ilya Sutskever, and Geoffrey E Hinton. Imagenet classification with deep convolutional neural networks. *Advances in neural information processing systems*, 25:1097–1105, 2012. 6
- [19] Xiaodong Kuang, Jianfei Zhu, Xiubao Sui, Yuan Liu, Chengwei Liu, Qian Chen, and Guohua Gu. Thermal infrared colorization via conditional generative adversarial network. *Infrared Physics & Technology*, 107:103338, 2020. 6, 7, 8, 10
- [20] Pierre-Yves Laffont, Zhile Ren, Xiaofeng Tao, Chao Qian, and James Hays. Transient attributes for high-level understanding and editing of outdoor scenes. *ACM Transactions on graphics (TOG)*, 33(4):1–11, 2014. 6

- [21] Hsin-Ying Lee, Hung-Yu Tseng, Jia-Bin Huang, Maneesh Singh, and Ming-Hsuan Yang. Diverse image-to-image translation via disentangled representations. In *Proceedings of the European conference on computer vision (ECCV)*, pages 35–51, 2018. 1, 2
- [22] Jae Hyun Lim and Jong Chul Ye. Geometric gan. *arXiv preprint arXiv:1705.02894*, 2017. 4, 5, 10
- [23] Yu Lin, Yigong Wang, Yifan Li, Yang Gao, Zhuoyi Wang, and Latifur Khan. Attention-based spatial guidance for image-to-image translation. In *Proceedings of the IEEE/CVF Winter Conference on Applications of Computer Vision*, pages 816–825, 2021. 3
- [24] Ming-Yu Liu, Thomas Breuel, and Jan Kautz. Unsupervised image-to-image translation networks. In *Advances in neural information processing systems*, pages 700–708, 2017. 1, 2
- [25] Jonathan Long, Evan Shelhamer, and Trevor Darrell. Fully convolutional networks for semantic segmentation. In *Proceedings of the IEEE conference on computer vision and pattern recognition*, pages 3431–3440, 2015. 3
- [26] Shuang Ma, Jianlong Fu, Chang Wen Chen, and Tao Mei. Da-gan: Instance-level image translation by deep attention generative adversarial networks. In *Proceedings of the IEEE Conference on Computer Vision and Pattern Recognition*, pages 5657–5666, 2018. 2
- [27] Sangwoo Mo, Minsu Cho, and Jinwoo Shin. Instagan: Instance-aware image-to-image translation. *arXiv preprint arXiv:1812.10889*, 2018. 2
- [28] Tim Salimans, Ian Goodfellow, Wojciech Zaremba, Vicki Cheung, Alec Radford, and Xi Chen. Improved techniques for training gans. *Advances in neural information processing systems*, 29:2234–2242, 2016. 6, 9
- [29] Andrew M Saxe, James L McClelland, and Surya Ganguli. Exact solutions to the nonlinear dynamics of learning in deep linear neural networks. *arXiv preprint arXiv:1312.6120*, 2013. 6
- [30] Zhiqiang Shen, Mingyang Huang, Jianping Shi, Xiangyang Xue, and Thomas S Huang. Towards instance-level image-to-image translation. In *Proceedings of the IEEE/CVF Conference on Computer Vision and Pattern Recognition*, pages 3683–3692, 2019. 1, 2, 6, 9
- [31] Jheng-Wei Su, Hung-Kuo Chu, and Jia-Bin Huang. Instance-aware image colorization. In *Proceedings of the IEEE/CVF Conference on Computer Vision and Pattern Recognition*, pages 7968–7977, 2020. 2
- [32] Wei Sun and Tianfu Wu. Image synthesis from reconfigurable layout and style. In *Proceedings of the IEEE/CVF International Conference on Computer Vision*, pages 10531–10540, 2019. 2, 5
- [33] Wei Sun and Tianfu Wu. Learning layout and style reconfigurable gans for controllable image synthesis. *arXiv preprint arXiv:2003.11571*, 2020. 6
- [34] Tristan Sylvain, Pengchuan Zhang, Yoshua Bengio, R Devon Hjelm, and Shikhar Sharma. Object-centric image generation from layouts. *arXiv preprint arXiv:2003.07449*, 1(2):4, 2020. 2
- [35] Hao Tang, Dan Xu, Nicu Sebe, and Yan Yan. Attention-guided generative adversarial networks for unsupervised image-to-image translation. In *2019 International Joint Conference on Neural Networks (IJCNN)*, pages 1–8. IEEE, 2019. 2
- [36] Ting-Chun Wang, Ming-Yu Liu, Jun-Yan Zhu, Andrew Tao, Jan Kautz, and Bryan Catanzaro. High-resolution image synthesis and semantic manipulation with conditional gans. In *Proceedings of the IEEE conference on computer vision and pattern recognition*, pages 8798–8807, 2018. 1, 2, 5
- [37] SHI Xingjian, Zhouong Chen, Hao Wang, Dit-Yan Yeung, Wai-Kin Wong, and Wang-chun Woo. Convolutional lstm network: A machine learning approach for precipitation nowcasting. In *Advances in neural information processing systems*, pages 802–810, 2015. 3
- [38] Richard Zhang, Phillip Isola, Alexei A Efros, Eli Shechtman, and Oliver Wang. The unreasonable effectiveness of deep features as a perceptual metric. In *Proceedings of the IEEE conference on computer vision and pattern recognition*, pages 586–595, 2018. 6
- [39] Bo Zhao, Lili Meng, Weidong Yin, and Leonid Sigal. Image generation from layout. In *Proceedings of the IEEE/CVF Conference on Computer Vision and Pattern Recognition*, pages 8584–8593, 2019. 1, 2, 6, 9
- [40] Yuzhi Zhao, Lai-Man Po, Kwok-Wai Cheung, Wing-Yin Yu, and Yasar Abbas Ur Rehman. Scgan: Saliency map-guided colorization with generative adversarial network. *IEEE Transactions on Circuits and Systems for Video Technology*, 2020. 2, 6, 7, 8, 10
- [41] Ziqiang Zheng, Yang Wu, Xinran Han, and Jianbo Shi. Forkgan: Seeing into the rainy night. In *Computer Vision—ECCV 2020: 16th European Conference, Glasgow, UK, August 23–28, 2020, Proceedings, Part III 16*, pages 155–170. Springer, 2020. 1
- [42] Jun-Yan Zhu, Taesung Park, Phillip Isola, and Alexei A Efros. Unpaired image-to-image translation using cycle-consistent adversarial networks. In *Proceedings of the IEEE international conference on computer vision*, pages 2223–2232, 2017. 1, 2
- [43] Jun-Yan Zhu, Richard Zhang, Deepak Pathak, Trevor Darrell, Alexei A Efros, Oliver Wang, and Eli Shechtman. Multi-modal image-to-image translation by enforcing bi-cycle consistency. In *Advances in neural information processing systems*, pages 465–476, 2017. 1, 2, 6, 7, 8, 9, 10